Environ Monit Assess (2025) 197:252
https://doi.org/10.1007/s10661-025-13705-3

RESEARCH

Investigating the effects of local climate zones on land surface temperature using spectral indices via linear regression model: a seasonal study of Sapanca Lake

Oznur Isinkaralar · Emmanuel Yeboah · Kaan Isinkaralar · Isaac Sarfo · Sevgi Öztürk · Dilara Yilmaz · Elias Bojago

Received: 2 July 2024 / Accepted: 24 January 2025 / Published online: 7 February 2025

Abstract The formation of urban heat islands is a widespread issue in cities. However, the impact of spectral indices on land surface temperature (LST) with various urban forms, climates, and functions has not been sufficiently examined. Currently, the prevalent method for analyzing complex urban areas is the classification of local climate zones (LCZs). In this study, we aim to explore the urban thermal environment by utilizing GIS-based spatial analyses and statistical methods. We also examine LCZs and the temporal-spatial changes of LSTs in Sapanca Lake and its surroundings. A comparative analysis was conducted on the relationship between the normalized difference vegetation index (NDVI), the modified normalized difference water index (MNDWI), and the normalized difference built-up index (NDBI) spectral indices in different LCZs and LST using a linear regression model. The results showed that all LCZs experienced a warming effect with an increase in NDBI, while they exhibited a cooling effect with the influence of NDVI and MNDWI. Notably, NDVI demonstrated a strong cooling effect in LCZ A (Dense trees) during the summer season, with an R^2 coefficient of 0.73. Similarly, MNDWI had an R^2 coefficient of 0.73 in LCZ A during spring. Values calculated as a result of regression are found as MAE:0.72 and MSE:0.75.

O. Isinkaralar · S. Öztürk
Department of Landscape Architecture, Faculty of Engineering and Architecture, Kastamonu University, 37150 Kastamonu, Türkiye
e-mail: obulan@kastamonu.edu.tr

S. Öztürk
e-mail: sozturk@kastamonu.edu.tr

E. Yeboah
School of Remote Sensing and Geomatics Engineering, Nanjing University of Information Science and Technology, Nanjing 210044, Jiangsu, China
e-mail: emmanuelyeboah@nuist.edu.cn

K. Isinkaralar (✉)
Department of Environmental Engineering, Faculty of Engineering and Architecture, Kastamonu University, 37150 Kastamonu, Türkiye
e-mail: kisinkaralar@kastamonu.edu.tr

I. Sarfo
College of Geography and Environmental Science, Henan University, Kaifeng, Henan Province, China
e-mail: isaacsarfo@henu.edu.cn

I. Sarfo
Organization of African Academic Doctors (OAAD), Off Kamiti Road, P. O. Box 25305000100, Nairobi, Kenya

D. Yilmaz
Department of Landscape Architecture, Graduate School of Natural and Applied Sciences, Kastamonu University, 37150 Kastamonu, Türkiye
e-mail: dlaraa.ylmaz@gmail.com

E. Bojago
Department of Environmental Science, College of Natural and Computational Sciences, Wolaita Sodo University, 138, Wolaita Sodo, Ethiopia
e-mail: eebojago@wsu.edu.et

These findings indicate the cooling effect of urban areas characterized by dense trees and water surfaces, highlighting their role in reducing LST. As a result, the research revealed the role of urban green systems and water surfaces in reducing the heat island effect, which is a problem, especially in urban centers. Overall, the study's results contribute to a better understanding of the thermal environmental characteristics in complex urban settings.

Keywords Climate risk · Remote sensing · Spectral indices · Spatiotemporal analysis · Urban heat island

Introduction

Over the past few decades, concerns about climate change on a global scale have increased worrying problems, and cities have great difficulty in adaptation processes. The 6th Assessment Report published by the Intergovernmental Panel on Climate Change (IPCC) in 2022 focuses on adaptation, adaptation processes, and vulnerability. According to the report, it is projected that by 2040, greenhouse gases present in the atmosphere and ongoing emission patterns will lead to more severe consequences than we experience today. The rise in carbon emissions and human-induced activities disrupt Earth's energy equilibrium and contribute to the degradation of our natural environment. According to Intergovernmental Panel on Climate Change (IPCC, 2022), this situation brings about significant transformations at both regional and global levels, including urban deforestation.

Urban heat island (UHI) problems occur due to urbanization, human activities, and built environment factors. The UHI effect worsens during heat waves and poses serious health issues (He, 2023; He et al., 2019; Heaviside et al., 2017). Rapid urbanization leads to converting natural vegetation and agricultural areas into impermeable surfaces, causing imbalances in land use. These transformations result in significant changes in the energy balance between urban surfaces and the atmosphere, leading to environmental and ecological problems (Isinkaralar & Isinkaralar, 2023). The increasing temperature effects of global climate change are becoming a matter of increasing concern worldwide, mainly because they can significantly affect the energy performance of buildings and indoor thermal comfort conditions (Kaitouni et al., 2023). Studies also investigate the impact of increasing temperatures on achieving the Sustainable Development Goals (SDGs), which aim to ensure a sustainable future (Howden-Chapman et al., 2017). The most significant sustainable development goal affected by abnormal changes in temperatures during the summer months is SDG 13-Climate Action. Increasing temperatures due to climate change and the effects have significant consequences on human and natural systems (Guven et al., 2024). Significant consequences such as the deterioration of residential areas, the danger of extinction of natural resource values, and the increase in poverty are significant enough to affect the whole world. At the same time, if these rising temperatures reach even more severe levels, they will prevent the achievement of SDG-2 No Hunger. As a result of the increase in temperatures, crop yield will be negatively affected, causing food shortages, malnutrition, and health problems it will bring, especially in vulnerable communities (Aydin et al., 2024; Isinkaralar et al., 2023). As a result of difficulty in accessing basic needs, problems will arise in achieving SDG-6 Clean Water. In addition, urban areas with poor infrastructure and vegetation are likely to experience even higher temperatures (Mahato et al., 2023).

Early studies have measured and evaluated UHI effects on different scales and critical planning and designing cities amidst climate stressors or the harsh conditions posed by extreme events. Land surface temperature (LST) is crucial when investigating UHI effects. Remote sensing (RS) and geographic information systems (GIS)-based analyses play an essential role in defining the LST model, as reported in several studies (Isinkaralar et al., 2024; Yao et al., 2023; Zhou et al., 2011). LULC indices (such as vegetation and construction) based on RS data are also used to examine LST changes in urban areas (Ramzan et al., 2022; Sharma & Joshi, 2016). Different terrain types significantly affect LST variations. Spectral indices obtained through RS-based analysis, which contain rich land cover information, play a significant role in determining this effect (Wang et al., 2018; Keerthi Naidu & Chundeli, 2023). Furthermore, developments in spectral indices have greatly facilitated mapping land use and land cover (LULC) (Santhosh & Shilpa, 2023). Regarding LST research, spectral indices are effective due to their easy application, lack of parameter requirements, and practical usability (Alexander, 2020; Mushore et al., 2022; Sun et al., 2016, 2017).

While several studies have examined the relationship between LST and spectral indices (Chen et al., 2020; Fan et al., 2019; Jenerette et al., 2016), most studies have focused on urban scale or land area. Some studies do not address the temporal process or provide sufficient data regarding findings and discussions due to the lack of diversity in land cover selection in sample areas. Also, investigating the relationship between LST and different urban forms and climate characteristics remains unexplored mainly or underdeveloped. The present study attempts to bridge this knowledge gap and explore this research opportunity, deeming it crucial to evaluate the relationship between spectral indices and LST in various urban areas, taking into account urban form, climate, and classification approaches (Wang & Ouyang, 2021). The local climate zone (LCZ) classification encompasses ten building types and seven land cover types, provides a valuable framework for characterizing urban landscapes, and is increasingly recognized as an essential factor influencing LST (Aslam & Rana, 2022).

Further, several research gaps and opportunities allay the investigation of LST parameters. First, seasonal LST differences have not been comprehensively addressed using the LCZ framework. While many studies have focused on urban areas with dense residential characteristics, there remains a lack of research on the LST effect in urban areas with dense urban vegetation. Urban vegetation is of great significance in reducing LST, one of the essential effects of climate change on cities (Wang, 2022). The present study investigates the seasonal dynamics between spectral indices and land surface temperature across urban morphologies, climatic contexts, and functional profiles.

Specifically, we attempted to analyze the relationship between the Normalized Difference Vegetation Index (NDVI), the Modified Normalized Difference Water Index (MNDWI), the Normalized Difference Built-up Index (NDBI), and LST in different LCZs, considering seasonal variations. On this basis, our research seeks to answer the following questions:

(i) How can seasonal changes in LST and LCZs using RS and GIS depending on urban components be evaluated?
(ii) How can we statistically model the seasonal differences between spectral indices, LST, and different LCZs?

Material and method

Study area

The study area for this research is Sapanca Lake and its surroundings in the Sakarya (Adapazarı) province, Türkiye. The reason for selecting this area is its unique topographic features. The study area is approximately 31 m above sea level, with the land's altitude ranging from − 18 to 1722 m. Sakarya province has a surface area of 4823 km^2, and Sapanca Lake has a surface area of 45 km^2. The elevation increases as one progresses towards the forested areas, in contrast to the declining altitude observed in the agricultural and residential zones.

Sapanca Lake, a case study, is mainly known for its natural beauty and topographic features formed through tectonic formations. Another noteworthy aspect of the area is the density of residential areas in and around Sapanca Lake. If it moves towards the lake's northeastern direction, it will find a higher concentration of residential and agricultural areas (Fig. 1).

The study domain has a warm and temperate climate. According to the Köppen-Geiger climate classification, the hottest month in the study area in Cfa is August, while the coldest month is December. It became a province on June 17, 1954. According to 2022 TÜİK data, its population is 281,489 people. Of the population, 49.63% are male and 50.37% are female. The agricultural and industrial sectors are essential in the province's economy. According to the development research conducted in 2022, the province ranks 87th in the second stage of socio-economic development. According to 2022 land use data, the province has 18% water, 44% forest, 14% crops, 9% built area, and 15% rangeland.

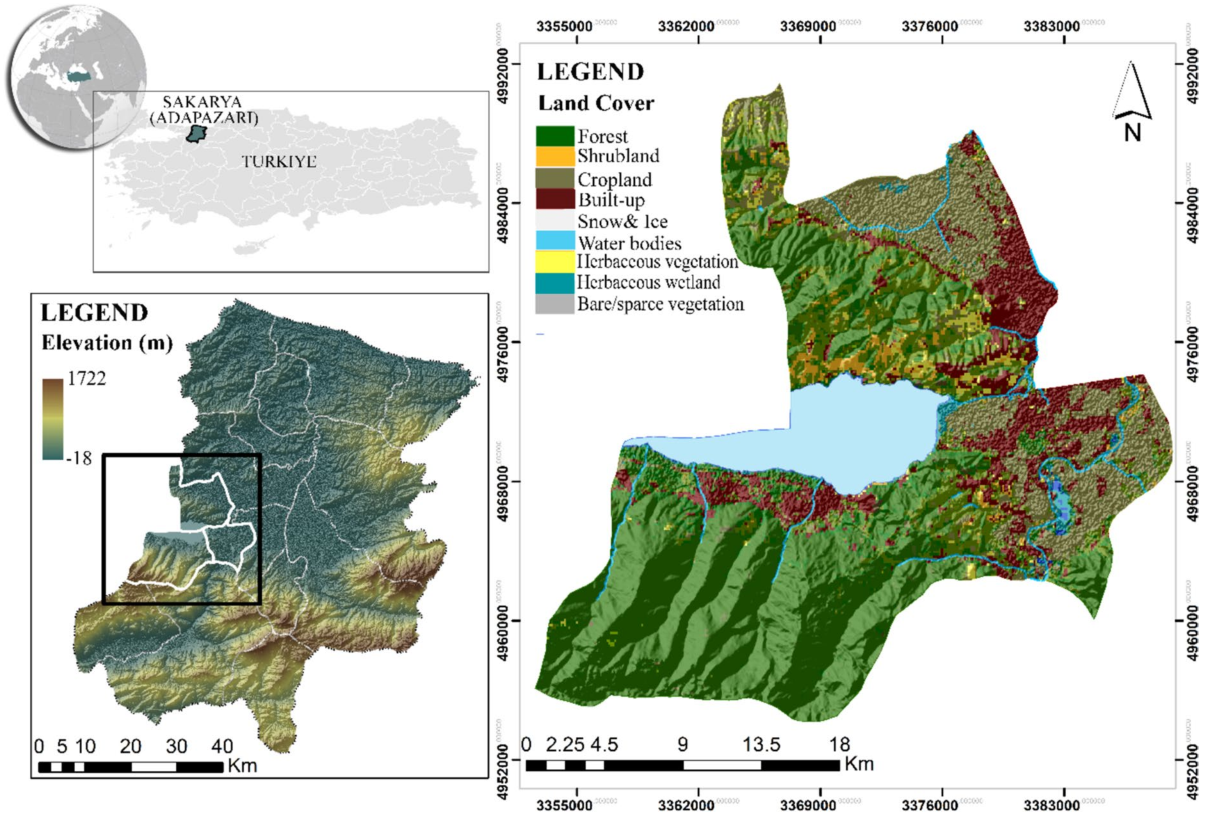

Fig. 1 Location map of the study area

Methodology

The study consists of three main stages. Firstly, data on remote sensing and satellite images were collected. Satellite images were derived from the United States Geological Survey (USGS) database. High resolution, low cloudiness 30*30 Landsat 8 OLI/TIRS satellite images representing the study area in four seasons were downloaded in GeoTIFF format. Then, LCZ and seasonal LST maps were created with the ArcGIS 10.4.1 program in Fig. 2. The accuracy of the maps was tested by calculating kappa statistics. Then, seasonal spectral indices were calculated. Finally, seasonal analysis of LST features with LCZs and spectral indexes was made by comparing them.

Data collection and processing

The conduct of this research, which aims to evaluate seasonal changes in LST and LCZs, has certain stages. The data collection and processing phase consists of two main parts: (i) classification of LCZs and (ii) seasonal LST.

Classification of LCZs The LCZ typology, developed by Stewart and Oke (2012), is a universal urban classification system. It categorizes urban areas based on a comprehensive understanding of the combination of micro-scale land covers and associated physical features. Unlike other land use/land cover schemes, the LCZ scheme focuses explicitly on urban and rural landscape types, which can be described using any of the 17 classes within the LCZ scheme. One of this scheme's significant advantages is its wide range of urban classes, capturing the diverse surface forms and land functions within urban areas. Furthermore, these classes are easily interpretable and globally consistent. The LCZ classes (Yoo et al., 2020) can be seen in Fig. 3.

To create the LCZ map of the study area, we first obtained data on building information, including building height (BH), pervious surface, impervious surface, and land cover. Building data was sourced from the

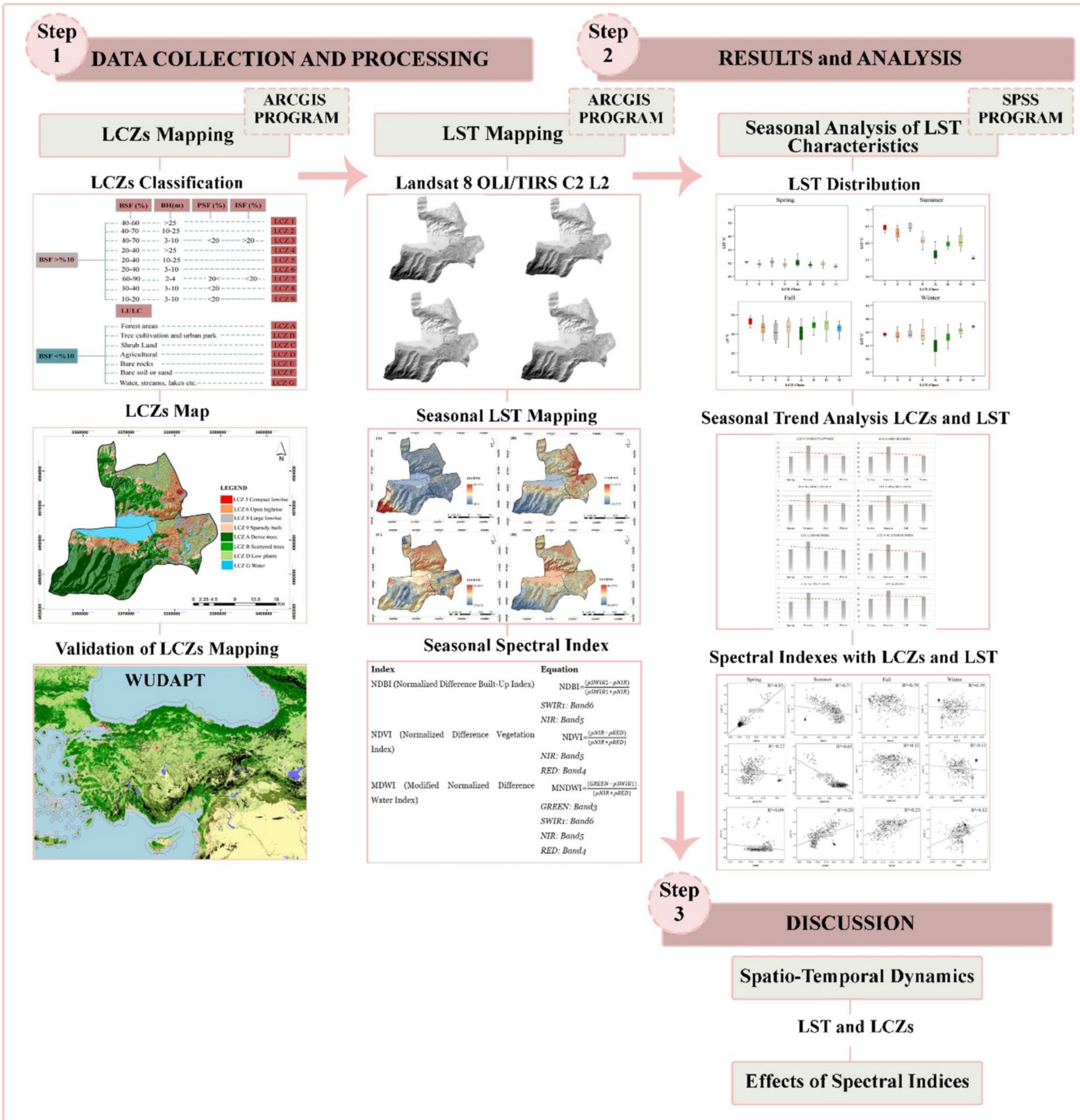

Fig. 2 The workflow steps of this study

database as an extension of Open Street Map. The BHs were obtained from the Copernicus Land Monitoring Service database. At the same time, land cover data were collected from the Copernicus Land Monitoring Service and Esri Land Cover—ArcGIS Living Atlas database. Next, we calculated the Building Surface Fractions (BSF), Pervious Surface Fractions (PSF), Impervious Surface Fractions (ISF), and Heights of Buildings. The methods and formulas (Eqs. 1–4) used for these computations can be found in Table 1. We then employed a GIS-based mapping method for further analysis.

After the data acquisition phase was completed, GIS-based classification and mapping techniques were used to classify LCZs based on the LCZ classification. The building data obtained in vector format was converted to raster data format in the ArcGIS 10.4.1 program.

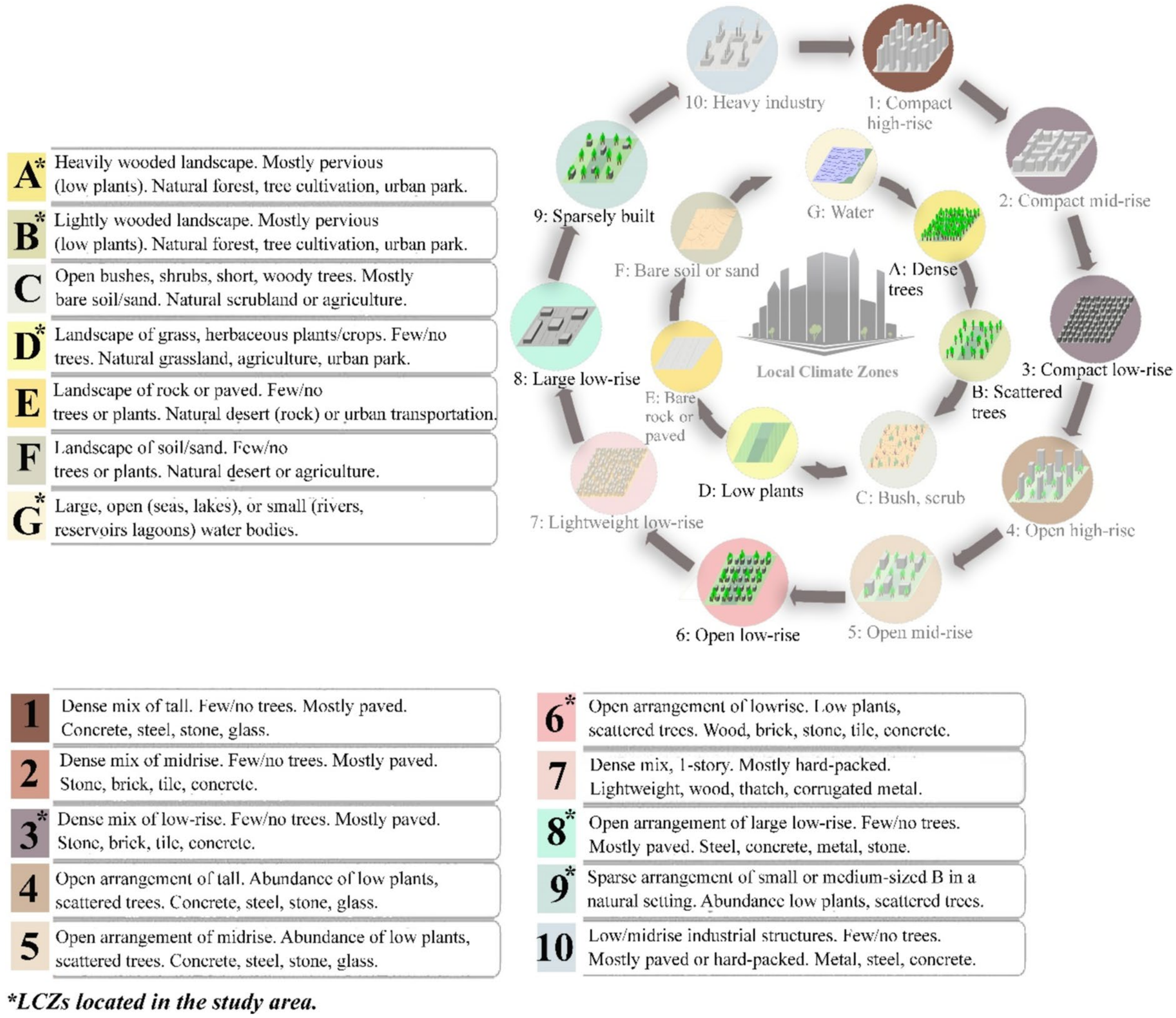

Fig. 3 LCZ classification

LCZ classification operations were performed using raster data. After all the data was obtained, the LCZ map was created using the raster calculator/mosaic process. LCZ classification stages are given in Fig. 4.

Validation of LCZ mapping World Urban Database Access Portal (WUDAPT) is used to determine the accuracy of the LCZ map. There are some biases in the analyses performed with satellite images. In order to avoid these errors, it is preferred that the satellite images to be used in LST calculations have the lowest cloud cover and the highest resolution value following the purpose and method of the study (Hodges et al., 2000; Martí-Cardona et al., 2019; Sattari et al., 2022). The WUDAPT database created enables comparative analyses. The accuracy assessment compares the LCZ map created with various analyses and tests with the WUDAPT data (Demuzere et al., 2022). The LCZ Generator provides interactive access to a global 100-m resolution map of Local Climate Zones, generated from multiple earth observation datasets and expert LCZ class labels. The LCZ scheme is a universal urban typology that can holistically distinguish urban areas based on the typical combination of micro-scale land covers and associated physical features. This approach differs from other land use/land cover schemes by focusing on both urban and rural landscape types, encompassed within the 17 LCZ classes. The key

Table 1 Description of physical parameters, data, and computation methods used in classifying LCZs

Parameters	Data	Definition	Equation
BSF	Building data	The ratio of building plan area to total plan area (%)	$BSF = \frac{\sum_{i=1}^{n} Bfa}{Ta} \times 100 \ldots (1)$ Bfa: Building footprint area n: The total number of buildings in the area Ta: Total area
BH	Building data Copernicus Land Monitoring Service data	Average of building heights (m)	$BH = \frac{\sum Tbh}{Tb} \ldots (2)$ TBH: The total building height Tb: The total number of buildings in the area
PSF	Land Cover data	The ratio of the previous plan area (bare soil, vegetation, water) to total plan area (%)	$PSF = \frac{\sum_{i=1}^{n} PSAi}{Ta} \times 100 \ldots (3)$ PSA: The area of pervious surface Ta: Total area
ISF	Land Cover data	The ratio of impervious plan area (paved, rock) to total plan area (%)	$ISF = (1 - (BSF + PSF)) \times 100 \ldots (4)$

Fig. 4 LCZ classification matrix

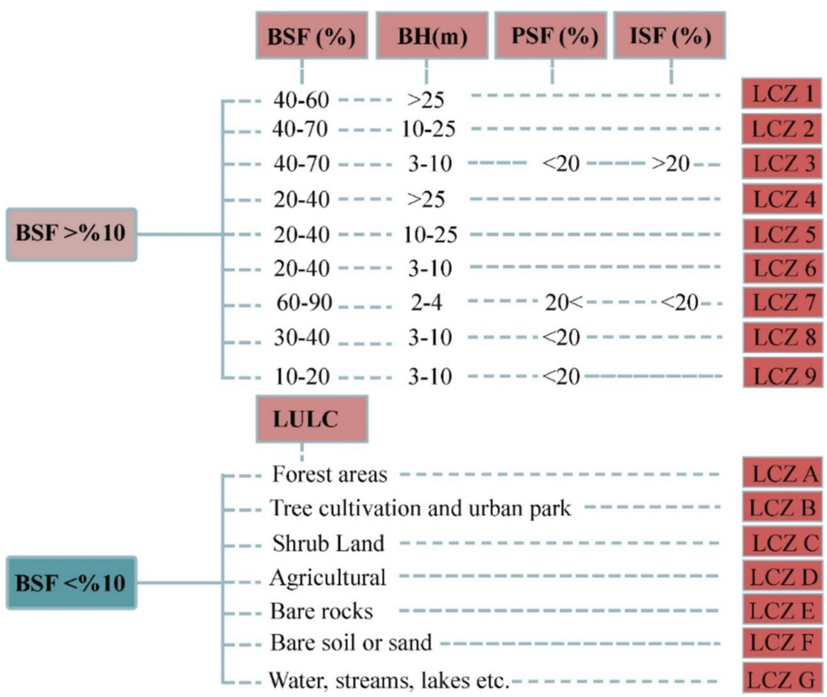

added value of the LCZ scheme is its ability to capture the diversity of urban classes, which represent the intra-urban variability of surface forms and land functions, in an easily interpretable and globally consistent manner (Guerri et al., 2021; Yang et al., 2020). The accuracy of the LCZ classification was assessed using a confusion matrix. The overall classification accuracy was 88.87%, with a kappa coefficient of 0.79, as recommended by Bechtel et al. (2015) as appropriate quality control metrics. According to the confusion matrix values presented in Table 2, the user's accuracy for LCZ 8 and LCZ B ranged from 61.74 to 83.97%.PA values range between 55 and 83.30%. The fact that the UA and PA values of the LCZ classes are generally close to each other shows that the classification is acceptable.

Seasonal LST To ensure accuracy, the dates of the satellite images were selected based on the climate

Table 2 LCZ transfer matrix of the study area

LCZs	3	6	8	9	A	B	D	G
3	61	15	1	0	0	0	0	0
6	15	68	0	0	3	5	7	1
8	1	0	7	0	0	0	0	0
9	0	0	0	72	0	7	6	0
A	0	3	0	0	48	2	0	0
B	0	5	0	7	2	53	32	0
D	0	7	0	6	0	32	51	0
G	0	1	0	0	0	0	0	15
UA (%)	78.98	83.97	57.54	61.74	83.12	59.35	79.74	71.71
PA (%)	83.30	76.65	55	56.94	81.50	62.29	70.60	82.80
Overall accuracy (%)	88.87							
Kappa	0.79							

characteristics of the study area. The satellite images used were dated as follows: 08.05.2022 for spring, 04.08.2022 for summer, 08.11.2022 for fall, and 08.01.2022 for winter. Notably, the LCZ and land use data are from 2022; therefore, satellite images from the same year were used to create the LST map. The workflow to generate the land surface temperature maps involved utilizing ArcGIS 10.4.1 and the 10th Landsat 8 satellite imagery band. The specific steps undertaken are as follows (Barsi et al., 2014; Roy et al., 2020): The data from the 10th band of the Landsat 8 OLI satellite image was converted into spectral radiance values using Eq. 5:

$$L_{\lambda} = \mathrm{ML} * \mathrm{Qcal} + \mathrm{AL} \tag{5}$$

The TOA spectral radiance was calculated using the equation Lλ = ML * QCal + AL, where ML represents the Radiance Mult Band, QCal denotes the quantized and calibrated standard product pixel values for Band 10, and AL stands for the Radiance Add Band. All of this information was obtained from the meta-data associated with the satellite imagery.

Subsequently, the temperature values were computed from the brightness values of the images using Eq. 6.

$$T = \frac{K_2}{In(\frac{K1}{L\lambda} + 1)} - 273.15 \tag{6}$$

where T: temperature degree (in Celsius), K_2: K_2 constant band(10), K_1: K_1 constant band(10), L_{λ}: spectral radiance. All of this information is obtained from the meta-data file of satellite images.

Next, an NDVI analysis was conducted following the temperature calculation. NDVI was computed using Bands 4 and 5 of the Landsat 8 satellite imagery, as described by Eq. 7.

$$\mathrm{NDVI} = \frac{(\mathrm{Band5} - \mathrm{Band4})}{(\mathrm{Band5} + \mathrm{Band4})} \tag{7}$$

In formulas, Bands 4 and 5 represent satellite image bands.

Following the NDVI analysis, the vegetation cover percentage is determined. This value is derived from the NDVI analysis. An equation was used to calculate the vegetation cover ratio.

$$\mathrm{PV} = \left(\frac{(NDVI - NDVI\mathrm{min})}{(NDVI\mathrm{max} - NDVI\mathrm{min})}\right)2 \tag{8}$$

where Pv represents the vegetation cover rate, NDVI is the normalized difference vegetation index, and $\mathrm{NDVI}_{\mathrm{min}}$ and $\mathrm{NDVI}_{\mathrm{max}}$ are the minimum and maximum values in the NDVI analysis, respectively.

Following the calculation of the vegetation ratio, the LSE analysis was then conducted using the subsequent algorithm.

$$\varepsilon = 0.004 * \mathrm{PV} + 0.986 \tag{9}$$

The land surface emissivity, denoted as ε, is calculated using the vegetation rate, PV, as a key parameter. Following this step, the final part of the land surface temperature analysis was conducted using the corresponding equation

$$LST = \frac{T_B}{\left(1 + \frac{\lambda * T_B}{\rho}\right) * In(\varepsilon)} \tag{10}$$

where T_B represents the temperature in degrees, λ denotes the spectral radiance wavelength, ρ is calculated as hc/s = 1.43888*10^{-2}mK = 14,388 mK, h is Planck's constant (6.626*10^{-34} Js), s is the Boltzmann constant (1.38*10^{-23} J/K), c is the velocity of light (2.998*10^{8} m/s = 14,388), and ε signifies the land surface emissivity.

Selected spectral indices NDBI, NDVI, and MDWI were used as spectral indices, and the expressions (Eqs. 11–13) used in measuring indices were presented in Table 3.

Seasonal analysis of LST features with LCZs and spectral indices

Comparative analyses of LST values were evaluated in four different sections: (1) First, seasonal LST values were evaluated comparatively within the scope of maps made in the ArcGIS 10.4.1; (2) The relationship between Seasonal LST and LCZs was analyzed by creating box-plot graphics in the SPSS 23 program; (3) The trend analysis of LST on LCZs was evaluated with the help of graphs created in the SPSS 23 program; and (4) Linear regression model (LRM) was performed to specify the relationship between LST, LCZs and spectral indices. Land cover features are one of the most important components affecting LST. Since the indices have different strengths and values in mapping land surface features, they are important for LST estimation. In this study, while selecting variables, linear regression analysis was performed to model the relationship between one or more explanatory variables when comparing the seasonal LST in the calculated LCZ regions with the land cover indices (NDBI, NDVI, and MNDWI) and to analyze these relationships by comparing them with R^2 coefficients. Findings about these comparative analyses are captured under the results and analysis section.

Spatial distribution results and analysis of LCZ

LCZ map

The distribution of LCZs in the study area is given in Fig. 5. When looking at the spatial distribution of LCZs, it can be observed that LCZ 6, representing one of the built-up types, as well as LCZ A, LCZ B, and LCZ G, which are land surface types, occupy more space than other LCZ types taking into account the results generated. After the calculations, the study area was classified within eight LCZ classifications: LCZ 3, LCZ 6, LCZ 8, LCZ 9, LCZ A, LCZ B, LCZ D and LCZ G. In the center of the area is LCZ G Water, while LCZ A Dense trees surround the north and south. On the south coast and west, the density of LCZ 9 Sparsely built covers a remarkable surface.

The area covered by LCZ types in the study area is LCZ 6 (13.85%), LCZ 9 (11.23), LCZ 8 (2.93%), and LCZ 3 (0.66), respectively. In land surface types, the areas covered by LCZ types are LCZ A (36.08%), LCZ D (13.35), LCZ B (12.28), and LCZ G (9.63%), respectively (Table 4).

Table 3 The spectral indexes, data, and calculation methods

Index	Data	Equation
NDBI	Remote sensing data (Landsat 8)	NDBI=$\frac{(\rho SWIR1-\rho NIR)}{(\rho SWIR1+\rho NIR)}$ … (11); SWIR1: Band6, NIR: Band5
NDVI		NDVI = $\frac{(\rho NIR-\rho RED)}{(\rho NIR+\rho RED)}$ … (12); NIR: Band5 RED: Band4
MDWI		MNDWI = $\frac{(GREEN-\rho SWIR1)}{(\rho NIR+\rho RED)}$ … (13); GREEN: Band3; SWIR1: Band6; NIR: Band5; RED: Band4

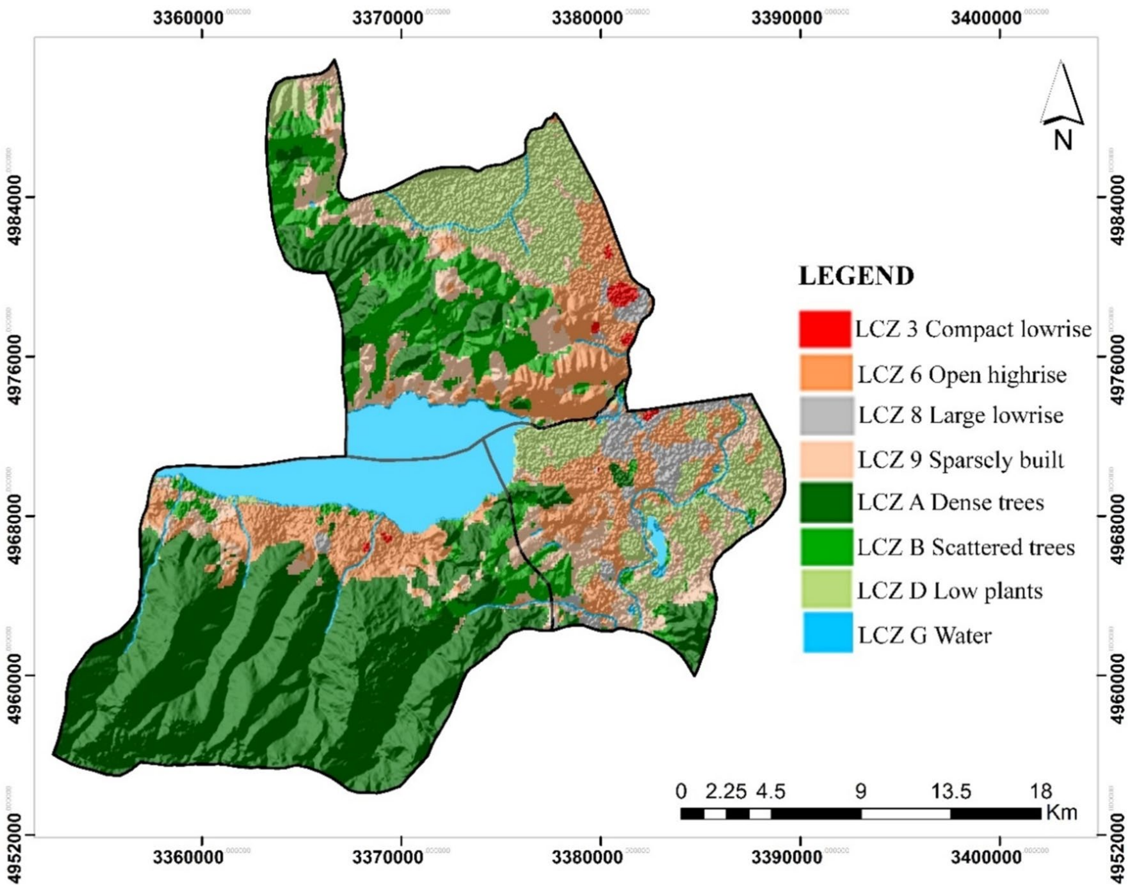

Fig. 5 LCZ map of the study area

Seasonal LST mapping

Figure 6 explains the spatial distribution of LST during different seasons. In that order, the highest LST values are observed in the summer, followed by fall, spring, and winter. Urban areas exhibit the highest LST values in autumn and summer, while forest areas and water surfaces exhibit the lowest LST values.

Table 5 provides the average LST values. The summer season has the highest average value, while the spring season has the lowest. When considering the spatial distribution of LST values in the spring season, there is only a 9.71 °C difference between the temperature values. This finding indicates that the values are very similar and align with the expectation of being at their lowest this season.

Table 4 The area of different LCZs types in the study area

	LCZ Types	Area (ha)	Percentage value (%)
Built types	LCZ 3 compact lowrise	433	0.66
	LCZ 6 open highrise	9140	13.85
	LCZ 8 large lowrise	1934	2.93
	LCZ 9 sparsely built	7413	11.23
Land cover types	LCZ A dense trees	23,813	36.08
	LCZ B scattered trees	8103	12.28
	LCZ D low plants	8808	13.35
	LCZ G water	6356	9.63

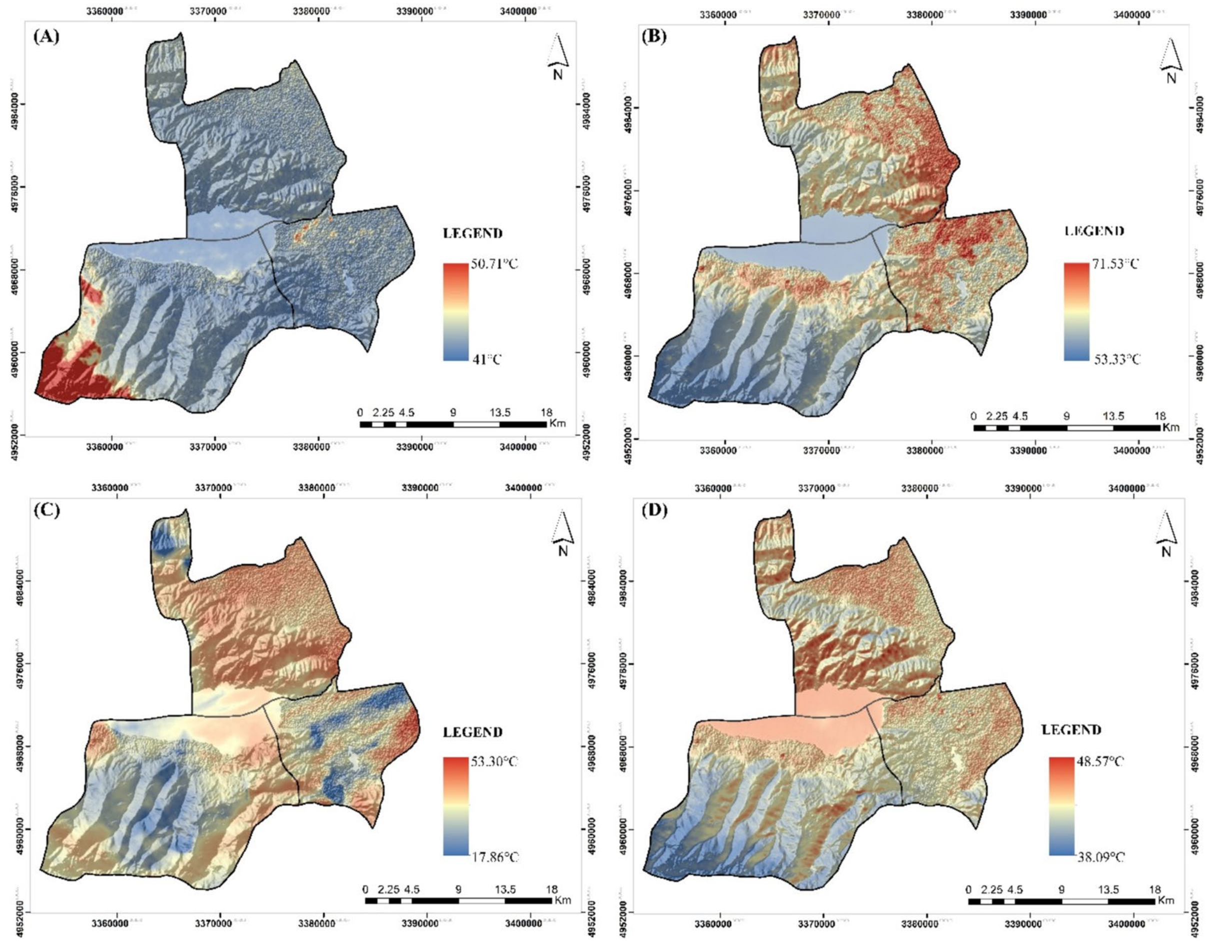

Fig. 6 LST variations during different seasons in the study area (**A** spring, **B** summer, **C** fall, **D** winter)

Table 5 Seasonal LST values (°C) of the study area

Seasons	Min	Max	Mean	SD
Spring	41	50.71	42.06	±1.02
Summer	53.33	71.53	59.03	±3.47
Fall	17.86	53.30	42.20	±2.54
Winter	38.09	48.57	43.13	±1.87

SD standard deviation

Seasonal LST with LCZs

Figure 7 depicts the seasonal variation in land surface temperature values for each local climate zone type, as represented by box plots. The findings demonstrate significant seasonal fluctuations in LST values across the different LCZ types. The summer months consistently exhibit the highest LST values, followed by fall and winter. Conversely, the lowest LST values are observed during the spring season. When comparing all LCZs, LCZ 3 and LCZ 8 display the highest temperature values in the summer, while LCZ A has the lowest in the fall.

Table 6 presents the LST values of various LCZ types in different seasons. The findings indicate that during the summer months, when temperatures are at their highest, LCZ 8 (64.55 °C) and LCZ 3 (64.99 °C) exhibit the highest average LST values. Following this, LCZ 6 (62.39 °C) and LCZ 9 (60.98 °C) are ranked accordingly. On the other hand, areas with dense trees, low vegetation, and water surfaces show the lowest LST values throughout the seasons. This

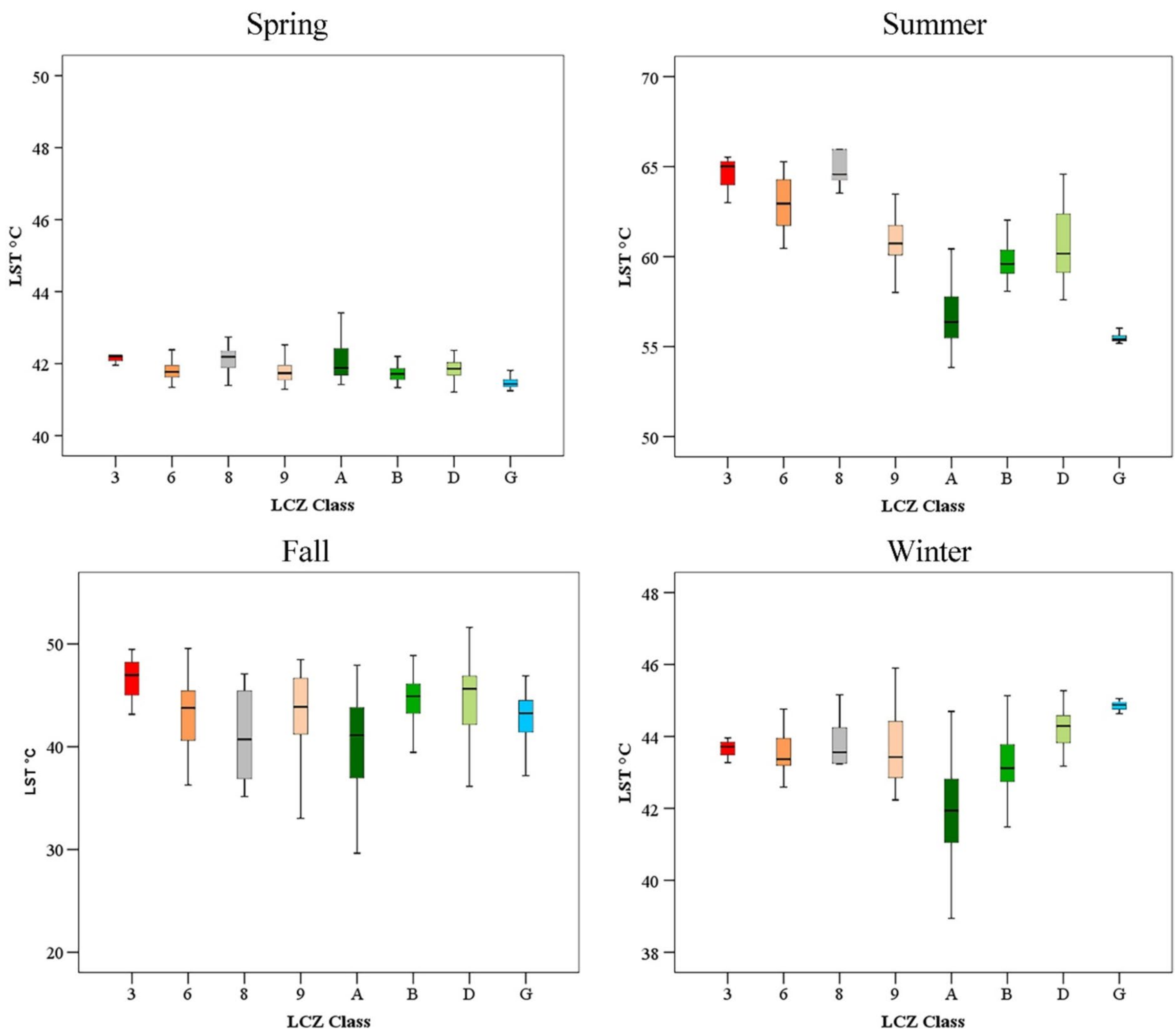

Fig. 7 Box-plot diagram of LST values of different LCZs during different seasons

Table 6 LST of different LCZs during different seasons (°C)

LCZ types		Spring		Summer		Fall		Winter	
		Range	Mean	Range	Mean	Range	Mean	Range	Mean
Built Types	LCZ 3	41.16–43.69	41.94	58.98–68.94	64.99	21.90–50.32	45.48	40.23–45.79	43.56
	LCZ 6	41–48.11	41.78	56.11–69.28	62.39	20.38–52.25	42.07	40.48–47.83	43.42
	LCZ 8	41.01–45.59	41.93	57.57–71.53	64.55	22.34–52.37	42.07	40.15–48.48	43.52
	LCZ 9	41.03–48.41	41.74	56.08–68.73	60.98	20.01–52.98	43.27	39.63–47.84	43.69
Land Cover Types	LCZ A	41.16–50.71	42.59	53.33–64.37	56.62	17.86–52.13	40.51	38.09–46.32	41.83
	LCZ B	41.06–50.58	41.76	55.48–67.67	59.88	20.44–52.38	43.99	39.68–47.34	43.64
	LCZ D	41.11–45.89	41.91	55.61–67–49	60.75	23.33–53.30	44.07	41.33–47.44	44.16
	LCZ G	41.10–42.95	41.46	55.05–63.24	55.55	24–47.54	42.52	42.52–46	44.76

LCZ 3 compact lowrise, *LCZ 6* open highrise, *LCZ 8* large lowrise, *LCZ 9* sparsely built, *LCZ A* dense trees, *LCZ B* scattered trees, *LCZ D* low plants, *LCZ G* water

result highlights the heat-absorbing nature of green surfaces.

Past research has shown that the LCZ scheme, a universal urban typology, is effective in distinguishing temperature variations across distinct urban landscape types. Specifically, prior studies have demonstrated that urban areas characterized by compact highrise, compact midrise, large lowrise, and heavy industrial land uses generally exhibit the highest land surface temperatures.

Seasonal trend analysis of LST over LCZs in Sapanca

Monitoring LST changes and trends is generally done in two different ways thus: (i) comparisons made with satellite images taken within a certain period (such as 5 or 10 years), and (ii) comparisons made with satellite images taken during a given season (i.e., spring, summer, autumn, winter). Within the scope of this study, a comparative analysis was made between the 2022 seasonal LST and LCZs of Sapanca Lake and its surroundings. Temperature data of 2022 the lake and its surroundings were considered in selecting the satellite image for LST trend determination.

Graphs for trend analysis of LST values in LCZs are depicted in Fig. 8. When examining the graphs, the elevated LST values during the spring and summer seasons in all LCZs stand out. Furthermore, the trend lines reveal a significant decline in LST values from the spring to winter seasons in LCZ 3, LCZ 6, and LCZ A. This decrease is mainly influenced by the low tree density, particularly in LCZ A.

The association of spectral indices against LCZs and LST

Maps of these spectral indices that are relevant to explaining the urban context with surface temperature values are given in Fig. 9. There are seasonal differences in NDVI, MNDWI, NDBI, and LST values.

The findings of the LRM between spectral indices and LST values are given in Fig. 10. The most substantial positive relationship between NDVI and LST is observed in spring, with an R^2 of 0.85. This positive relationship is followed by the fall season with R^2 values of 0.79, summer with 0.81, and winter with 0.19. On the other hand, the relationship between MNDWI and LST is consistently negative across all seasons. The most significant negative impact is seen in the summer season, with an R^2 value of 0.65, while the winter season has the least negative impact, with an R^2 value of 0.11. Generally, the relationship between NDBI and LST shows low R^2 values. This result is because there are more forest areas and water surfaces in the study area. However, except for spring, the relationship between NDBI and LST is consistently negative, suggesting a negative impact on LST values.

NDVI plays a crucial role in representing vegetation and significantly reduces LST through transpiration and shading. The cooling effect of NDVI varies across different LCZs and shows seasonal differences. Generally, as temperature values decrease, the cooling effect in LCZs decreases during the spring and summer seasons. LCZ A exhibits the most potent cooling effect of NDVI in the summer, with a negative R^2 value of 0.73. MNDWI, on the other hand, is an essential parameter in reducing LST through evaporation. It possesses high heat capacity and low thermal conductivity. The highest impact of MNDWI on LCZs is observed in LCZ 3 during the spring season, with a negative R^2 value of 0.97. The effect of MNDWI is more pronounced in LCZs (3–9) compared to LCZs (A–G). NDBI serves as an index for determining built-up areas. It has a more significant heating effect in all LCZs, primarily during the spring and summer. LCZ 6 exhibits the most substantial heating effect of NDBI during the spring season, with an R^2 value of 0.98. Conversely, LCZ B shows the lowest heating effect during winter, with an R^2 value of 0.09 (Table 7).

Discussion

Spatiotemporal dynamics of LST within local climate regions

The Sapanca Lake area and its surroundings provide a valuable opportunity for studying the characteristics of LST to land cover. Various factors, such as water surfaces, forests, buildings, and vegetation, significantly influence LST in this study area. The changes in the study area over the years reveal the necessity of precautions. Critical temporal warming, especially in the northern part of the area, is spatially highlighted in Fig. 11.

Particularly during the summer, areas with high residential density experience elevated LST.

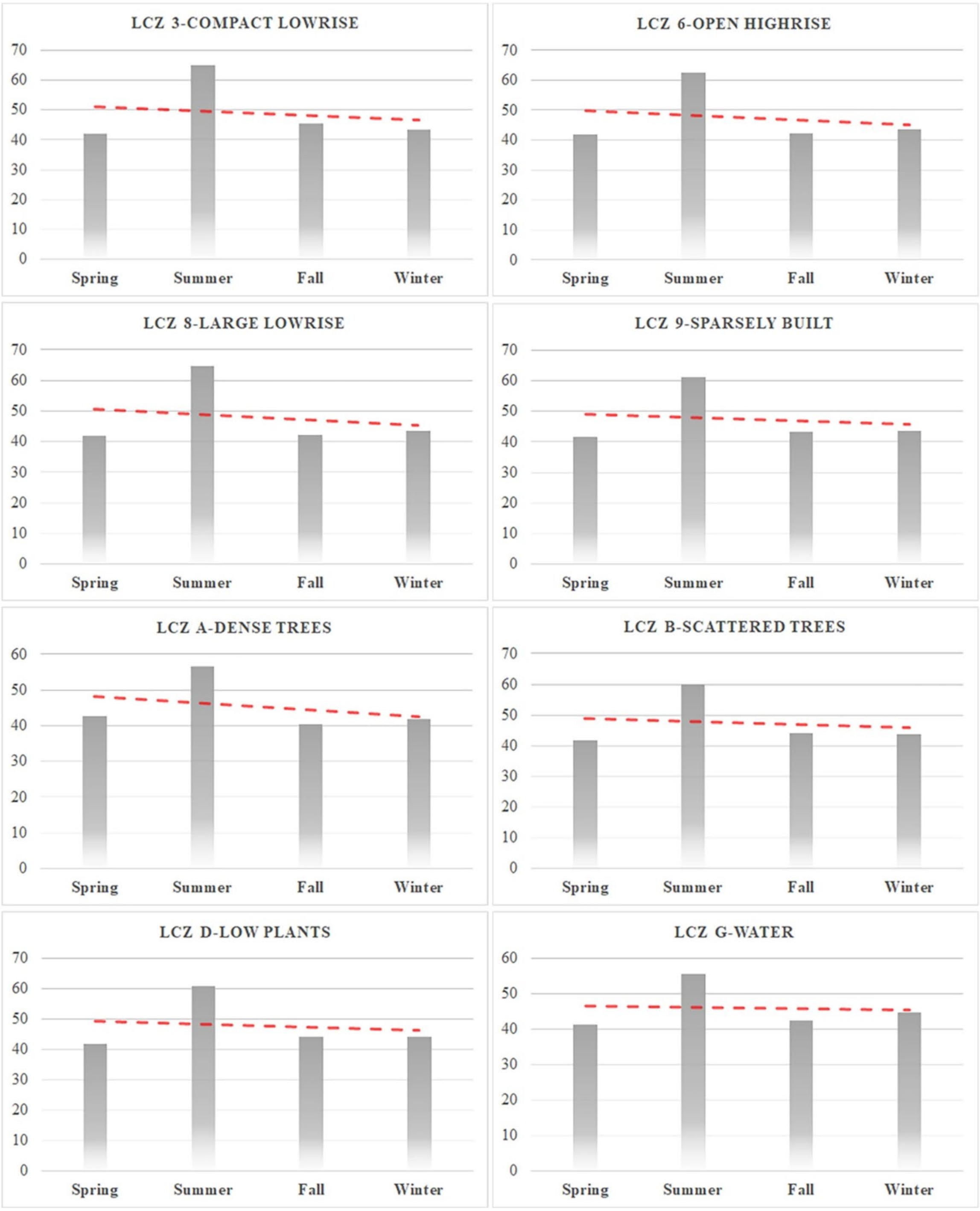

Fig. 8 Seasonal trend analysis of LST in LCZs

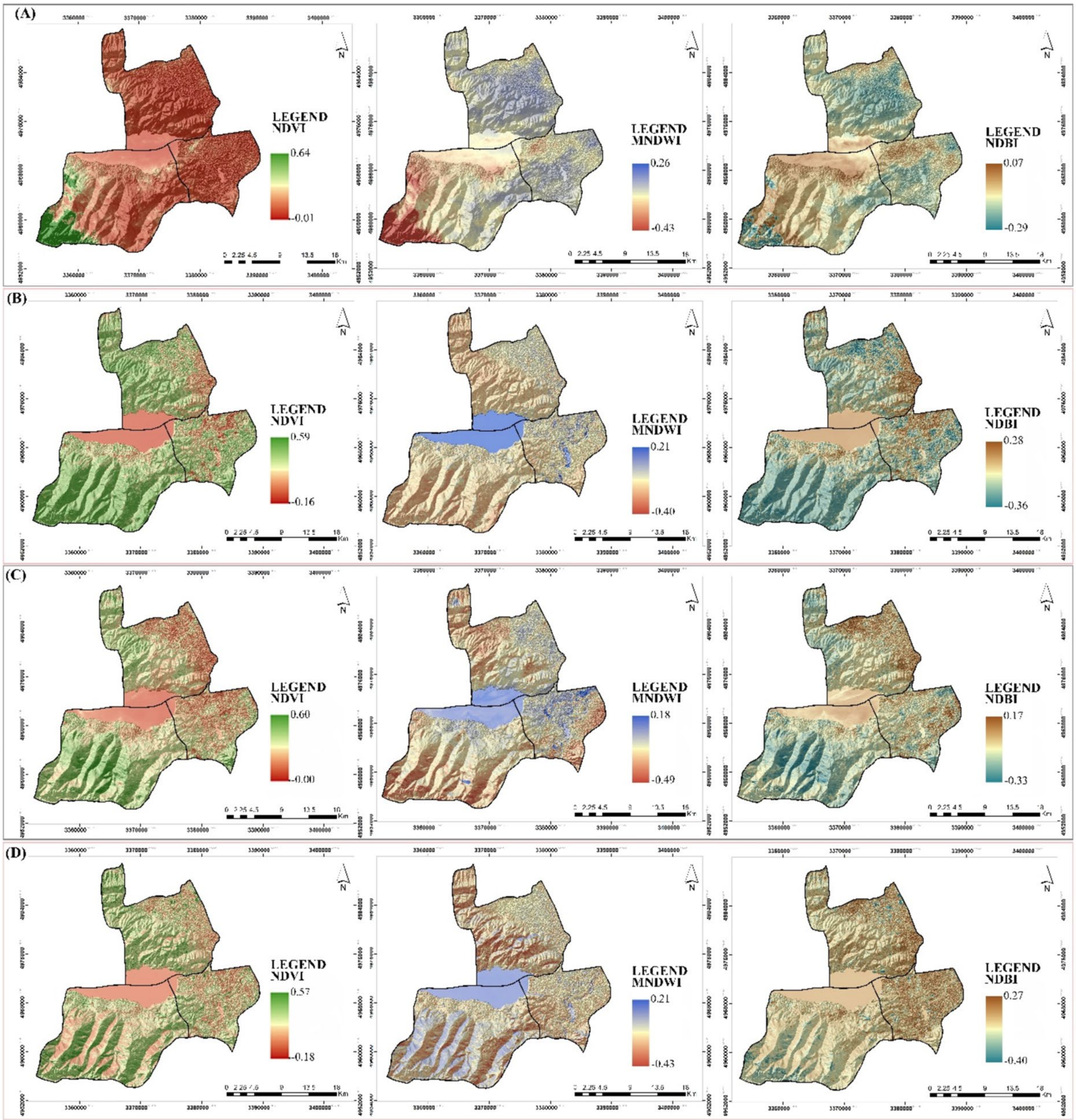

Fig. 9 Maps of spectral indices (**A** spring, **B** summer, **C** fall, **D** winter)

However, it is worth noting that water surfaces and woodland regions have a cooling effect, as indicated by seasonal variations in LST. LST is a crucial indicator of climate change, and its variations across regions can be attributed to factors such as vegetation cover, urbanization, and topography (Yu et al., 2018). Understanding these temporal-spatial changes is vital for predicting future climate trends and implementing effective mitigation strategies. Figure 6 explores the spatial distribution of LST in different seasons. The highest LST value is observed in the summer, followed by autumn, spring, and winter. The regional distribution of LST reveals a distinct pattern of temperature variation throughout the year. Seasonal variations in LST levels can be called solar radiation, vegetation cover,

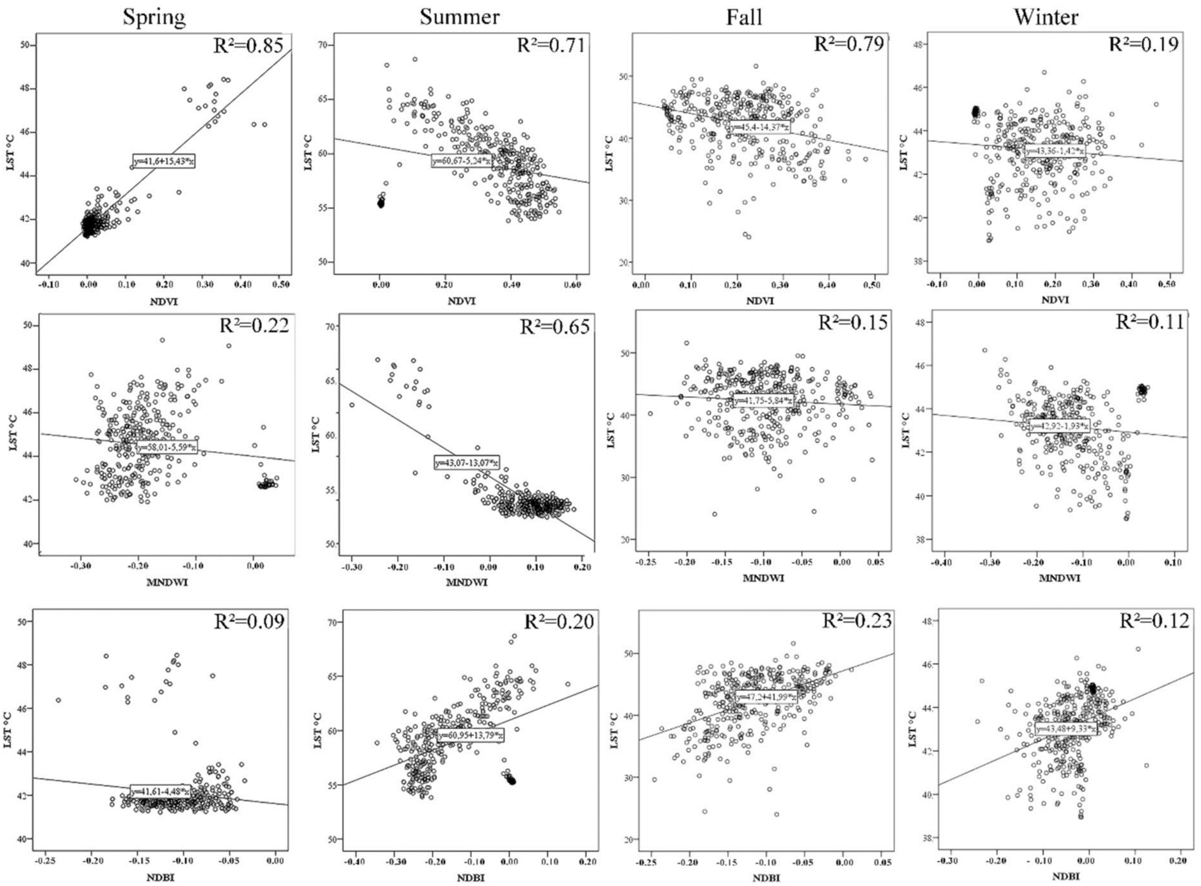

Fig. 10 The LRM between spectral indexes and LST

and urban heat island effects. During the fall and summer, urban areas exhibit the highest LST values, while forests and water surfaces have the lowest (Yuan & Bauer, 2007). These findings align with the research by Han et al. (2023), which discovered that high-value LST zones were predominantly observed on impermeable surfaces.

In contrast, low-value LST regions were more concentrated in water and forest areas such as the Qiantang River, West Lake, Xixi Wetland, and Gaoting Mountain. Overall, the regional distribution of LST provides valuable insights into the impact of various environmental conditions on temperature fluctuations. This information is essential for understanding local climate patterns and informing urban planning and land use decisions. The LCZ map was created to distinguish between surface temperatures in the research area. Previous studies in different regions have found that the highest LST is generally observed in LCZ 1 (compact highrise buildings), LCZ 2 (compact, medium buildings), LCZ 8 (large lowrise buildings), and LCZ Z (heavy industry) regions, as studies suggest (Wang et al., 2019; Zhao et al., 2021). In this study, it was discovered that LCZ 3 (compact lowrise buildings), LCZ 6 (open highrise buildings), LCZ 8 (large lowrise buildings), and LCZ 9 (sparsely built areas) had the highest LSTs, and it was determined that temperature values varied significantly depending on the season. However, building height, density, and land cover all significantly impact the intensity of the UHI.

Moreover, research is needed to investigate the specific factors underlying these temperature changes across metropolitan zones. While LCZ 3 (compact lowrise buildings) stands out for its high summer temperatures, LCZ G (water) stands out

Table 7 Seasonal average spectral index values and LRM coefficients (R^2) in different LCZs

LCZ Types		NDVI				MNDWI				NDBI			
		Sp	S	F	Wi	Sp	S	F	Wi	Sp	S	F	Wi
LCZ 3 compact lowrise	M_v	0.01	0.11	0.09	0.06	0.10	−0.17	−0.07	−0.12	−0.11	0.23	−0.05	0.04
	R^2	0.55**	0.21*	0.66*	0.33**	0.97*	0.67*	0.59**	0.76*	0.95**	0.47**	0.46**	0.43**
LCZ 6 open highrise	M_v	0.01	0.24	0.16	0.13	0.08	−0.18	−0.07	−0.13	−0.1	−0.08	−0.1	−0.02
	R^2	0.48**	0.36*	0.13*	0.11*	0.30*	0.36*	0.38*	0.20*	0.98**	0.97**	0.51**	0.97**
LCZ 8 large lowrise	M_v	0	0.13	0.12	0.08	0.1	−0.14	−0.06	−0.11	−0.1	−0.03	−0.09	0
	R^2	0.08**	0.10*	0.50*	0.21**	0.18*	0.13**	0.25**	0.09**	0.23**	0.21**	0.30**	0.69**
LCZ 9 sparsely built	M_v	0.01	0.32	0.21	0.17	0.1	−0.2	−0.11	−0.16	−0.12	−0.13	−0.11	−0.04
	R^2	0.28**	0.59*	0.29*	0.10**	0.25*	0.12**	0.26*	0.34*	0.38**	0.46**	0.42**	0.20**
LCZ A dense trees	M_v	0.06	0.43	0.28	0.18	0.03	−0.21	−0.12	−0.11	−0.1	−0.21	−0.15	−0.07
	R^2	0.88**	0.73*	0.13*	0.22**	0.81*	0.13**	0.34*	0.31*	0.79*	0.29*	0.19**	0.14*
LCZ B scattered trees	M_v	0.01	0.38	0.24	0.2	0.1	−0.22	−0.11	−0.18	−0.13	−0.17	−0.12	−0.04
	R^2	0.08**	0.41*	0.11*	0.15**	0.02*	0.03**	0.20*	0.39*	0.08*	0.39**	0.22**	0.09**
LCZ D low plants	M_v	0	0.33	0.16	0.13	0.11	−0.16	−0.09	−0.12	−0.12	−0.17	−0.08	−0.02
	R^2	0.39**	0.54*	0.08*	0.30**	0.30**	0.09**	0.10*	0.20**	0.10**	0.59**	0.29**	0.16**
LCZ G water	M_v	0.01	0.01	0.06	−0.01	0.06	0.03	0	0.03	−0.07	0.01	−0.06	0
	R^2	0.24**	0.83**	0.43*	0.31*	0.17*	0.11*	0.03**	0.51**	0.12**	0.73*	0.26**	0.10*

Note 1: the asterisks ** and * refer to positive and negative correlations

Note 2: M_v mean value, *Sp* spring, *S* summer, *F* fall, *Wi* winter

in the autumn and winter. These findings indicate that urban planning and design significantly influence local temperatures and should be considered in future development efforts. Additionally, studying the thermal properties of different land cover types in metropolitan areas could provide valuable insights for minimizing the impacts of heat islands.

Effects of spectral indices on LST and LCZs

NDVI and LST exhibited a negative correlation during summer ($R^2=0.73$), indicating that as vegetative health improves, surface temperatures decrease. This finding is reinforced by Huang et al. (2024), who found that increased vegetation leads to more excellent absorption of solar radiation, resulting in higher surface temperatures. Similarly, Sun et al. (2022) discovered that higher vegetation levels increase vegetation transpiration and evaporation, leading to higher atmospheric water vapor content and increased surface precipitation. The significant negative correlation suggests a strong association between these two variables during this period. Consequently, the correlation between NDVI and LST is significantly weaker in autumn and spring compared to summer and winter, as indicated by the degrees. This result highlights the importance of monitoring vegetation health to understand its impact on surface temperature fluctuations throughout the year.

Further research could explore how these findings can be applied to enhance agricultural practices and mitigate climate change (Wang, 2021). Greenness is closely linked to rainfall, and increased vegetation greenness reduces surface temperature through shading, evapotranspiration, and photosynthesis. Therefore, the influence of vegetation greenness on LST is more pronounced in the spring. As a result, the study concludes that vegetation growth restricts LST.

The study found that specific spectral indices, including NDVI, MNDWI, and NDBI, significantly impact LST and can help distinguish different LCZs. The cooling effect of NDVI in LCZs decreased during the spring and summer seasons as temperature values dropped. This finding is consistent with the research of Sun and Kafatos (2007), who found that NDVI reduces LST in warmer seasons and amplifies it during colder seasons, with a significant negative relationship between LST and NDVI only observed during warm seasons. These findings suggest that

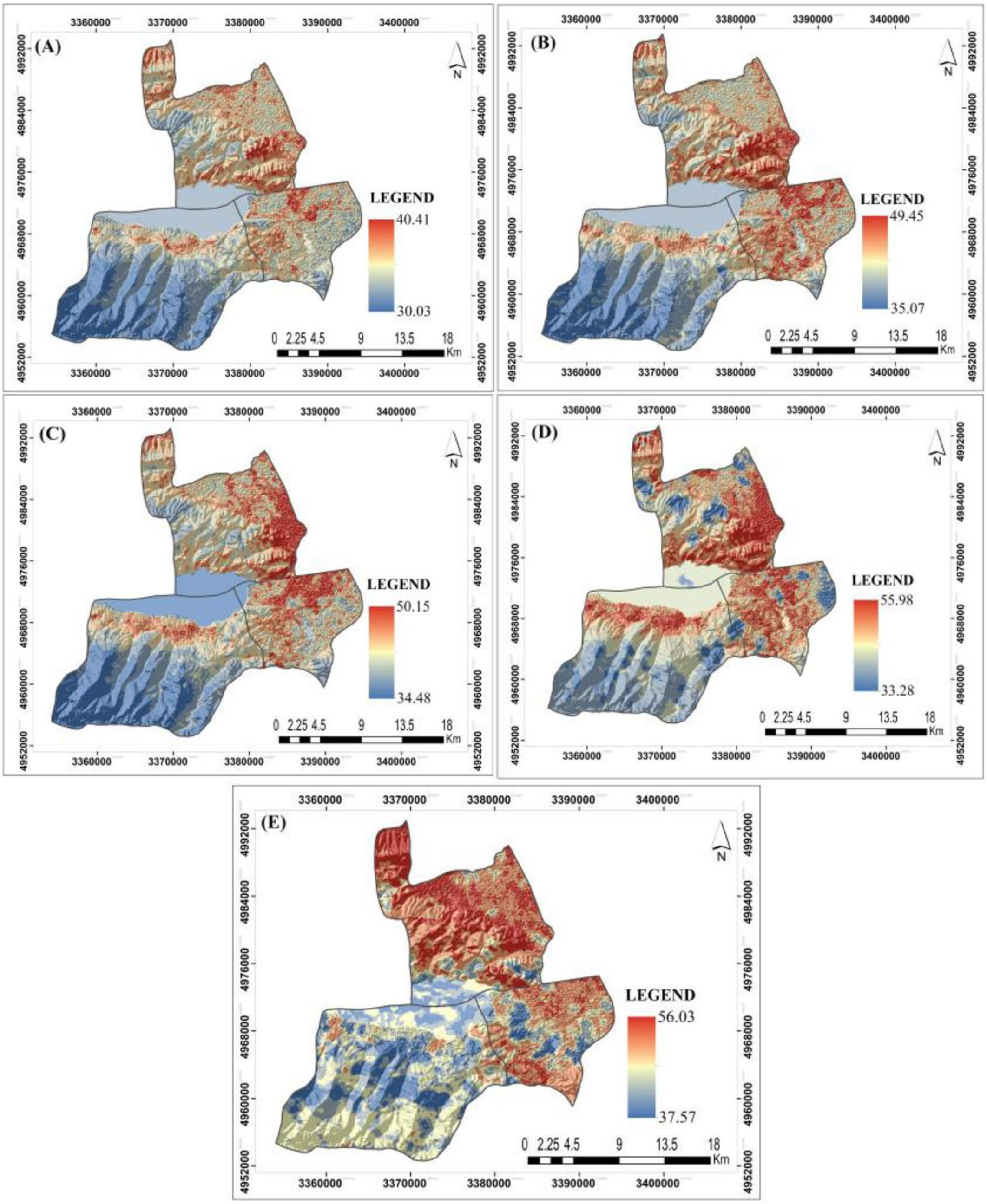

Fig. 11 Spatiotemporal change of LST maps of Sapanca **A** 1990, **B** 2000, **C** 2010, **D** 2020, and **E** 2022

monitoring these spectral indices can ensure a valuable perception of the effects of urban heat islands and inform urban planning strategies to mitigate heat stress in different LCZs (He et al., 2021; Mokarram et al., 2023). The study investigates the relationship between spectral indices and changes in LST over time. LCZ A demonstrates the most effective cooling during hot weather.

This data has the potential to provide valuable insights to city planners, enabling them to make well-informed decisions regarding the design of urban areas. By understanding the correlation between spectral indices and temperature fluctuations, cities can effectively develop tailored strategies to counteract the urban heat island effect in different LCZs. The findings of this study highlight the significant cooling effect that forests exhibit during the hottest months of the year, which is consistent with the observations made by Yin et al. (2022). According to their research, forests can have a remarkable cooling impact of up to 8.4 °C during the study period. Furthermore, statistical data suggests that integrating more green spaces and vegetation into urban development can help alleviate the consequences of escalating temperatures. Moreover, these findings support the critical importance of preserving and expanding forested areas within cities to create a more sustainable and pleasant environment for residents.

From the LCZ 3 perspective, it has the most decisive impact on MNDWI and LCZs during spring. LCZ 3, characterized by compact midrise buildings and limited vegetation, offers the most tremendous potential for reducing the urban heat island effect. Implementing green infrastructure, such as parks, green roofs, and street trees, in these areas, according to Sarfo et al. (2023), could significantly lower temperatures and enhance urban residents' quality of life. The influence of MNDWI on LST values is more pronounced in LCZs (3–9) than in LCZs (A–G). This suggests that targeting LCZs 3–9 for water-based interventions may be more effective in mitigating the urban heat island effect than LCZs A–G. Additionally, incorporating water features like ponds and wetlands in these regions could enhance cooling effects and improve livability. The warming effect of NDBI is more excellent in all LCZs, especially during the spring and summer seasons, compared to other seasons.

Focusing on minimizing NDBI in all LCZs, particularly during warmer months, can help reduce the urban heat island effect and improve thermal comfort for people. Solutions like green roofs and reflecting pavements can also lower surface temperatures and create a more sustainable urban environment. When adopting urban heat island mitigation techniques, it is essential to consider land cover features. By prioritizing LCZ 3–9 and incorporating water features, cities can effectively lower temperatures and improve residents' well-being. Understanding seasonal variations in the warming effects of NDBI can guide targeted interventions during high-risk periods. Urban blue-green areas play a crucial role in reducing LST. The results of this study are based on Xiang et al. (2023) and Mo et al. (2024), and are consistent in their work. These results underscore the importance of integrating blue-green infrastructure with well-designed urban morphology to mitigate the UHI phenomenon. Analyzing these metrics can enhance understanding of urban heat island impacts and inform urban planning approaches to alleviate heat-related stress. Recognizing the moderating influence of natural geographic features on temperature is crucial for climate change mitigation and urban planning and design. A comprehensive systems-level perspective is required, especially in developing urban green infrastructure. To ensure balance, water bodies and permeable surfaces should be carefully planned and distributed. This comprehensive approach should consider factors such as the size, distribution, and connectivity of green spaces and the integration of water management systems like ponds, wetlands, and permeable pavements. Careful planning and implementation of these elements can help mitigate urban heat island effects and create more resilient, livable cities in the face of climate change.

Conclusion

This paper aimed to develop an evaluation approach for a comprehensive dual evaluation of the UHI effect. The method integrates LST and spectral indices based on LCZ classification to assess the UHI phenomenon in detail. UHI is a significant concern in urban areas. In areas with complex urban morphology and climatic characteristics, it is insufficient to solely investigate the effect of spectral indices on LST. Analysis of LST's temporal and spatial variations based on LCZ is also fundamental in detecting that temperature varies between different LCZs. Therefore, this study provided a valuable basis for urban planning by seasonally evaluating the relationship between spectral indices and LST within different LCZs. Urban planning measures are critical, primarily since it is known that urbanization is held responsible for the concern caused by the climate crisis worldwide. This relationship was examined using a LRM. In addition, the LRM used is based on the hypothesis of a linear association between the indices and LST. It was found that all LCZs exhibited a warming effect with an increase in the Normalized Difference Built-up Index (NDBI). However, the NDVI and MNDWI showed a cooling effect when impacted. The most potent cooling effect of NDVI was observed in LCZ A, with a coefficient of determination (R^2) value (0.73) during the summer season.

On the other hand, the most potent cooling effect of MNDWI was observed in LCZ 3, with an R^2 of 0.97 in the spring season. This may be attributed to the high density of LCZ 3 zones around the largest wetland in the study area. The results obtained from this study can provide essential recommendations for urban planners and policymakers in their efforts to improve thermal comfort in urban areas.

Limitations and future research directions

As satellite imagery becomes increasingly prevalent across diverse research domains, comprehending the limitations and potential biases associated with data acquisition timing has emerged as a crucial consideration in ensuring the validity and reliability of the resulting analyses. Satellite remote sensing offers high spatial resolution but often suffers from limited temporal coverage, with images captured at specific time points that may not align with research objectives or the natural cycles and variations within the study area. Furthermore, the selection and timing of image collection can significantly impact the quality and accuracy of land cover mapping and change detection, as factors such as vegetation phenology, cloud cover, and solar illumination can fluctuate considerably across seasons. Consequently, researchers must exercise caution in accounting for these seasonal factors when analyzing satellite-derived land cover data, as they can introduce significant bias into the interpretation of land cover changes and the detection of long-term trends or patterns. Similarly, this study has some limitations. Firstly, the satellite images used in this study represent the LST values observed at 08:39 in the morning, as the Landsat satellite passed over the study area during this time. Another limitation is that due to the satellite image's features, such as resolution and cloudiness, it was impossible to calculate thirty-day LST values in seasonal analyses. Due to distortions in the images, one-day LST values representing the current month were used in the analyses and evaluations by the climatic conditions of the study area in seasonal analyses. For future studies, it would be beneficial to analyze the spatial effects of LSTs in all LCZs throughout the day and night and during different seasons, using data obtained from satellites that cover different time zones. This would provide more comprehensive results. Numerous accuracy assessments and precision improvements have been made for the LCZ classification. In the scope of the study, the confusion matrix was calculated for the accuracy assessment, and the computed values show that the classification is acceptable. However, there is still a need to improve the cartographic accuracy of the LCZ classification and develop a unified/standard method for creating LCZ maps. The LCZ classification used in this analysis may have inaccuracies due to technical constraints and may not fully capture the actual urban landscape. Additionally, various factors at the city scale, such as building morphology, land cover characteristics, building material differences, population, and socio-economic conditions, can contribute significantly to the observed thermal environment. Consequently, the selection of the study area may impact the regression analysis. Therefore, future research should examine the relationship between LST and driving factors across different urban scales to derive more comprehensive conclusions. While the current study utilized relevant LULC indices, there are numerous other potential indicators that could be explored. Although the indices that best represent the urban context were preferred in the study, different indices such as normalized difference impervious index (NDISI), bare soil index (BI), urban index (UI), index-based built-up index (IBI), and enhanced built-up and bareness index (EBBI) can be used in future studies. This study evaluates the impact of LULC indices on seasonal LST in 2022. Future research on similar topics should consider the LULC indices utilized in this study as critical parameters for understanding LST variations in the urban setting. However, it is likely that additional indices may also significantly influence these temperature patterns. The effect of land cover on LST is inevitable. It is also important to determine this situation. Especially in seasonal analyses, determining the magnitude and direction of the effect of land cover on LST will facilitate the production of effective policies in the adaptation process to climate change. In statistics, linear regression is a linear approach used to model the relationship between a scalar response and one or more explanatory variables. This method, frequently used in climate studies, is important in determining the percentage level of the variables affecting LST. For this reason, linear regression analysis was performed in the study. However, due to the developments in statistical analyses, different methods like machine learning also provide effective results in climate studies. It will be beneficial to use different methods in future studies. Another limitation is that this study only evaluates a specific sample area within the urban area rather than considering the entire area. It is suggested that future research should analyze the impact of spectral indices on LCZ and LST in larger urban areas, which may yield different or similar results with higher or lower statistical values. At the same time, it is considered that using the evaluation method developed within the scope of the study will play an essential role in determining the parameters that will effectively reduce LST in studies conducted on a similar subject at different scales in different cities.

Author contribution OI: Processing analysis, interpretation, original draft, data curation. EY: Processing analysis, interpretation, original draft, data curation. KI: Processing analysis, interpretation, original draft, data curation. IS: Writing – review & editing. SÖ: Writing – review & editing: DY: Writing, data curation. EB: Writing – review & editing.

Data availability No datasets were generated or analysed during the current study.

Declarations

Ethics approval All authors have read, understood, and have complied as applicable with the statement on "Ethical responsibilities of Authors" as found in the Instructions for Authors.

Consent to participate Not applicable.

Consent for publication Not applicable.

Competing interests The authors declare no competing interests.

References

Alexander, C. (2020). Normalised difference spectral indices and urban land cover as indicators of land surface temperature (LST). *International Journal of Applied Earth Observation and Geoinformation, 86*, 102013. https://doi.org/10.1016/j.jag.2019.102013

Aslam, A., & Rana, I. A. (2022). The use of local climate zones in the urban environment: A systematic review of data sources, methods, and themes. *Urban Climate, 42*, 101120. https://doi.org/10.1016/j.uclim.2022.101120

Aydin, H., Yenigun, K., Isinkaralar, O., & Isinkaralar, K. (2024). Hydrological low flow and overlapped trend analysis for drought assessment in Western Black Sea Basin. Natural Hazards, 1–31. https://doi.org/10.1007/s11069-024-06880-y

Barsi, J., Schott, J., Hook, S., Raqueno, N., Markham, B., & Radocinski, R. (2014). Landsat-8 thermal infrared sensor (TIRS) vicarious radiometric calibration. *Remote Sensing, 6*(11), 11607–11626. https://doi.org/10.3390/rs61111607

Bechtel, B., Alexander, P. J., Böhner, J., Ching, J., Conrad, O., Feddema, J., ... & Stewart, I. (2015). Mapping local climate zones for a worldwide database of the form and function of cities. *ISPRS International Journal of Geo-Information*, *4*(1), 199–219. https://doi.org/10.3390/ijgi4010199

Chen, W., Zhang, J., Shi, X., & Liu, S. (2020). Impacts of building features on the cooling effect of vegetation in community-based MicroClimate: Recognition, measurement and simulation from a case study of Beijing. *International Journal of Environmental Research and Public Health, 17*(23), 8915. https://doi.org/10.3390/ijerph17238915

Demuzere, M., Kittner, J., Martilli, A., Mills, G., Moede, C., Stewart, D., ... & Bechtel, B. (2022). A global map of local climate zones to support earth system modelling and urban scale environmental science. *Earth System Science Data*, *14*(8), 1–57. https://doi.org/10.5194/essd-14-3835-2022

Fan, H., Yu, Z., Yang, G., Liu, T. Y., Liu, T. Y., Hung, C. H., & Vejre, H. (2019). How to cool hot-humid (Asian) cities with urban trees? An optimal landscape size perspective. *Agricultural and Forest Meteorology, 265*, 338–348. https://doi.org/10.1016/j.agrformet.2018.11.027

Guerri, G., Crisci, A., Messeri, A., Congedo, L., Munafò, M., & Morabito, M. (2021). Thermal summer diurnal hot-spot analysis: The role of local urban features layers. *Remote Sensing, 13*(3), 538. https://doi.org/10.3390/rs13030538

Guven, D. S., Yenigun, K., Isinkaralar, O., & Isinkaralar, K. (2024). Modeling flood hazard impacts using GIS-based HEC-RAS technique towards climate risk in Şanlıurfa, Türkiye. Natural Hazards, 1–19. https://doi.org/10.1007/s11069-024-06945-y

Han, S., Hou, H., Estoque, R. C., Zheng, Y., Shen, C., Murayama, Y., ... & Hu, T. (2023). Seasonal effects of urban morphology on land surface temperature in a three-dimensional perspective: A case study in Hangzhou, China. *Building and Environment, 228*, 109913. https://doi.org/10.1016/j.buildenv.2022.109913

He, B. J. (2023). Cause-related injustice, process-related injustice, effect-related injustice and regional heat action planning priorities: An empirical study in Yangtze River Delta and Chengdu-Chongqing urban agglomerations. *Landscape and Urban Planning, 237*, 104800. https://doi.org/10.1016/j.landurbplan.2023.104800

He, B. J., Wang, J., Liu, H., & Ulpiani, G. (2021). Localized synergies between heat waves and urban heat islands: Implications on human thermal comfort and urban heat management. *Environmental Research, 193*, 110584. https://doi.org/10.1016/j.envres.2020.110584

He, B. J., Zhao, Z. Q., Shen, L. D., Wang, H. B., & Li, L. G. (2019). An approach to examining performances of cool/hot sources in mitigating/enhancing land surface temperature under different temperature backgrounds based on Landsat 8 image. *Sustainable Cities and Society, 44*, 416–427. https://doi.org/10.1016/j.scs.2018.10.049

Heaviside, C., Macintyre, H., & Vardoulakis, S. (2017). The urban heat island: Implications for health in a changing environment. *Current Environmental Health Reports, 4*, 296–305. https://doi.org/10.1007/s40572-017-0150-3

Hodges, K. I., Chappell, D. W., Robinson, G. J., & Yang, G. (2000). An improved algorithm for generating global window brightness temperatures from multiple satellite infrared imagery. *Journal of Atmospheric and Oceanic Technology, 17*(10), 1296–1312. https://doi.org/10.1175/1520-0426(2000)017%3c1296:AIAFGG%3e2.0.CO;2

Howden-Chapman, P., Siri, J., Chisholm, E., Chapman, R., Doll, C. N., & Capon, A. (2017). SDG 3: Ensure healthy lives and promote well-being for all at all ages. A guide to SDG interactions: from science to implementation. Paris, France: International Council for Science, 81–126.

Huang, B., Huang, Y., Wu, D., Bao, X., Wu, Y., Feng, G., & Li, L. (2024). The influence of vegetation on climate elements in northwestern China. *Atmosphere, 15*(3), 325. https://doi.org/10.3390/atmos15030325

IPCC IPCC (Intergovernmental Panel on Climate Change). (2022). Climate Change 2022. https://www.ipcc.ch/report/ar6/wg2/

Isinkaralar, O., Isinkaralar, K., Yilmaz, D., & Öztürk, S. (2024). Multi-dimensional analysis of land use/land cover and urbanization on seasonal variation of land surface temperature in İzmir, Türkiye. *Landscape and Ecological Engineering*, 1–18. https://doi.org/10.1007/s11355-024-00628-3

Isinkaralar, O., & Isinkaralar, K. (2023). Projection of bioclimatic patterns via CMIP6 in the Southeast Region of Türkiye: A guidance for adaptation strategies for climate policy. *Environmental Monitoring and Assessment, 195*(12), 1448. https://doi.org/10.1007/s10661-023-11999-9

Isinkaralar, O., Isinkaralar, K., & Bayraktar, E. P. (2023). Monitoring the spatial distribution pattern according to urban land use and health risk assessment on potential toxic metal contamination via street dust in Ankara, Türkiye. *Environmental Monitoring and Assessment, 195*(9), 1085. https://doi.org/10.1007/s10661-023-11705-9

Jenerette, G. D., Harlan, S. L., Buyantuev, A., Stefanov, W. L., Declet-Barreto, J., Ruddell, B. L., ... & Li, X. (2016). Micro-scale urban surface temperatures are related to land-cover features and residential heat related health impacts in Phoenix, AZ USA. *Landscape Ecology*, *31*, 745–760. https://doi.org/10.1007/s10980-015-0284-3

Kaitouni, S. I., Chahboun, R., Bouhssine, Z., Cakan, M., Brigui, J., & Ahachad, M. (2023). Simulation-based assessment of the climate change impact on future thermal energy load and indoor comfort of a light-weight ecological building across the six climates of Morocco. *Thermal Science and Engineering Progress, 45*, 102137. https://doi.org/10.1016/j.tsep.2023.102137

Keerthi Naidu, B. N., & Chundeli, F. A. (2023). Assessing LULC changes and LST through NDVI and NDBI spatial indicators: A case of Bengaluru, India. *GeoJournal*, 1–16. https://doi.org/10.1007/s10708-023-10862-1

Mahato, S., Kundu, B., Makwana, N., & Joshi, P. K. (2023). Early summer temperature anomalies and potential impacts on achieving Sustainable Development Goals (SDGs) in National Capital Region (NCR) of India. *Urban Climate, 52*, 101705. https://doi.org/10.1016/j.uclim.2023.101705

Martí-Cardona, B., Prats, J., & Niclòs, R. (2019). Enhancing the retrieval of stream surface temperature from Landsat data. *Remote Sensing of Environment, 224*, 182–191. https://doi.org/10.1016/j.rse.2019.02.007

Mo, N., Han, J., Yin, Y., & Zhang, Y. (2024). Seasonal analysis of land surface temperature using local climate zones in peak forest basin topography: A case study of Guilin. *Building and Environment, 247*, 111042. https://doi.org/10.1016/j.buildenv.2023.111042

Mokarram, M., Taripanah, F., & Pham, T. M. (2023). Investigating the effect of surface urban heat island on the trend of temperature changes. *Advances in Space Research, 72*(8), 3150–3169. https://doi.org/10.1016/j.asr.2023.06.048

Mushore, T. D., Mutanga, O., & Odindi, J. (2022). Estimating urban LST using multiple remotely sensed spectral indices and elevation retrievals. *Sustainable Cities and Society, 78*, 103623. https://doi.org/10.1016/j.scs.2021.103623

Ramzan, M., Saqib, Z. A., Hussain, E., Khan, J. A., Nazir, A., Dasti, M. Y. S., ... & Niazi, N. K. (2022). Remote sensing-based prediction of temporal changes in land surface temperature and land use-land cover (LULC) in urban environments. *Land*, *11*(9), 1610. https://doi.org/10.3390/land11091610

Roy, S., Pandit, S., Eva, E. A., Bagmar, M. S. H., Papia, M., Banik, L., ... & Razi, M. A. (2020). Examining the nexus between land surface temperature and urban growth in Chattogram Metropolitan Area of Bangladesh using long term Landsat series data. *Urban Climate*, *32*, 100593. https://doi.org/10.1016/j.uclim.2020.100593

Santhosh, L. G., & Shilpa, D. N. (2023). Assessment of LULC change dynamics and its relationship with LST and spectral indices in a rural area of Bengaluru district, Karnataka India. *Remote Sensing Applications: Society and Environment, 29*, 100886. https://doi.org/10.1016/j.rsase.2022.100886

Sarfo, I., Bi, S., Xu, X., et al. (2023). Planning for cooler cities in Ghana: Contribution of green infrastructure to urban heat mitigation in Kumasi Metropolis. *Land Use Policy, 133*, 106842. https://doi.org/10.1016/j.landusepol.2023.106842

Sattari, F., Hashim, M., Sookhak, M., Banihashemi, S., & Pour, A. B. (2022). Assessment of the TsHARP method for spatial downscaling of land surface temperature over urban regions. *Urban Climate, 45*, 101265. https://doi.org/10.1016/j.uclim.2022.101265

Sharma, R., & Joshi, P. K. (2016). Mapping environmental impacts of rapid urbanization in the National Capital Region of India using remote sensing inputs. *Urban Climate, 15*, 70–82. https://doi.org/10.1016/j.uclim.2016.01.004

Stewart, I. D., & Oke, T. R. (2012). Local climate zones for urban temperature studies. *Bulletin of the American*

Meteorological Society, 93, 1879–1900. https://doi.org/10.1175/BAMS-D-11-00019.1

Sun, D., & Kafatos, M. (2007). Note on the NDVI-LST relationship and the use of temperature-related drought indices over North America. *Geophysical Research Letters*, *34*(24). https://doi.org/10.1029/2007GL031485

Sun, S., Liu, Y., Chen, H., Ju, W., Xu, C. Y., Liu, Y., ... & Yu, M. (2022). Causes for the increases in both evapotranspiration and water yield over vegetated mainland China during the last two decades. *Agricultural and Forest Meteorology*, *324*, 109118. https://doi.org/10.1016/j.agrformet.2022.109118

Sun, G. Y., Chen, X. L., Jia, X. P., Yao, Y. J., & Wang, Z. J. (2016). Combinational build-up index (CBI) for effective impervious surface mapping in urban areas. *IEEE Journal of Selected Topics in Applied Earth Observations and Remote Sensing, 9*, 2081–2092. https://doi.org/10.1109/JSTARS.2015.2478914

Sun, Z., Wang, C., Guo, H., & Shang, R. (2017). A modified normalized difference impervious surface index (MNDISI) for automatic urban mapping from Landsat imagery. *Remote Sensing, 9*(9), 942. https://doi.org/10.3390/rs9090942

Wang, L. (2022). Exploring a knowledge map for urban resilience to climate change. *Cities, 131*, 104048. https://doi.org/10.1016/j.cities.2022.104048

Wang, R., Cai, M., Ren, C., Bechtel, B., Xu, Y., & Ng, E. (2019). Detecting multi-temporal land cover change and land surface temperature in Pearl River Delta by adopting local climate zone. *Urban Climate, 28*, 100455. https://doi.org/10.1016/j.uclim.2019.100455

Wang, Y., Du, H., Xu, Y., Lu, D., Wang, X., & Guo, Z. (2018). Temporal and spatial variation relationship and influence factors on surface urban heat island and ozone pollution in the Yangtze River Delta, China. *Science of the Total Environment, 631–632*, 921–933. https://doi.org/10.1016/j.scitotenv.2018.03.050

Wang, Y., & Ouyang, W. (2021). Investigating the heterogeneity of water cooling effect for cooler cities. *Sustainable Cities and Society, 75*, 103281. https://doi.org/10.1016/j.scs.2021.103281

Wang, Z. H. (2021). Compound environmental impact of urban mitigation strategies: Co-benefits, trade-offs, and unintended consequence. *Sustainable Cities and Society, 75*, 103284. https://doi.org/10.1016/j.scs.2021.103284

Xiang, Y., Tang, Y., Wang, Z., Peng, C., Huang, C., Dian, Y., ... & Zhou, Z. (2023). Seasonal variations of the relationship between spectral indexes and land surface temperature based on local climate zones: A study in three Yangtze River megacities. *Remote Sensing*, *15*(4), 870. https://doi.org/10.3390/rs15040870

Yang, G., Yu, Z., Jørgensen, G., & Vejre, H. (2020). How can urban blue-green space be planned for climate adaption in high-latitude cities? A seasonal perspective. *Sustainable Cities and Society, 53*, 101932. https://doi.org/10.1016/j.scs.2019.101932

Yao, X., Zeng, X., Zhu, Z., Lan, Y., Shen, Y., Liu, Q., & Yang, F. (2023). Exploring the diurnal variations of the driving factors affecting block-based LST in a "Furnace city" using ECOSTRESS thermal imaging. *Sustainable Cities and Society, 98*, 104841. https://doi.org/10.1016/j.scs.2023.104841

Yin, S., Peng, L. L., Feng, N., Wen, H., Ling, Z., Yang, X., & Dong, L. (2022). Spatial-temporal pattern in the cooling effect of a large urban forest and the factors driving it. *Building and Environment, 209*, 108676. https://doi.org/10.1016/j.buildenv.2021.108676

Yoo, C., Lee, Y., Cho, D., Im, J., & Han, D. (2020). Improving local climate zone classification using incomplete building data and Sentinel 2 images based on convolutional neural networks. *Remote Sensing, 12*(21), 3552. https://doi.org/10.3390/rs12213552

Yu, Z., Xu, S., Zhang, Y., Jørgensen, G., & Vejre, H. (2018). Strong contributions of local background climate to the cooling effect of urban green vegetation. *Scientific Reports, 8*(1), 6798. https://doi.org/10.1038/s41598-018-25296-w

Yuan, F., & Bauer, M. E. (2007). Comparison of impervious surface area and normalized difference vegetation index as indicators of surface urban heat island effects in Landsat imagery. *Remote Sensing of Environment, 106*(3), 375–386. https://doi.org/10.1016/j.rse.2006.09.003

Zhao, Z., Sharifi, A., Dong, X., Shen, L., & He, B. J. (2021). Spatial variability and temporal heterogeneity of surface urban heat island patterns and the suitability of local climate zones for land surface temperature characterization. *Remote Sensing, 13*(21), 4338. https://doi.org/10.3390/rs13214338

Zhou, W., Huang, G., & Cadenasso, M. L. (2011). Does spatial configuration matter? Understanding the effects of land cover pattern on land surface temperature in urban landscapes. *Landscape and Urban Planning, 102*, 54–63. https://doi.org/10.1016/j.landurbplan.2011.03.009